

See discussions, stats, and author profiles for this publication at: <https://www.researchgate.net/publication/224019620>

Guiding Block Copolymers into Sequenced Patterns via Inverted Terrace Formation

ARTICLE *in* MACROMOLECULES · MARCH 2012

Impact Factor: 5.8 · DOI: 10.1021/ma202616w

CITATIONS

5

READS

59

6 AUTHORS, INCLUDING:



Sungjune Park

RWTH Aachen University

8 PUBLICATIONS 32 CITATIONS

[SEE PROFILE](#)



Larisa Tsarkova

RWTH Aachen University

56 PUBLICATIONS 682 CITATIONS

[SEE PROFILE](#)



Stefan Roitsch

University of Cologne

26 PUBLICATIONS 277 CITATIONS

[SEE PROFILE](#)



Alexander Böker

Fraunhofer Institute for Applied Polymer Rese...

139 PUBLICATIONS 4,699 CITATIONS

[SEE PROFILE](#)

Guiding Block Copolymers into Sequenced Patterns via Inverted Terrace Formation

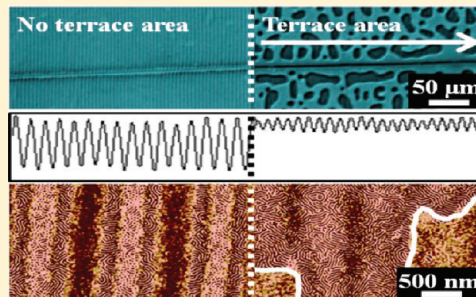
Sungjune Park,[†] Larisa Tsarkova,^{*,†} Stephanie Hiltl,[†] Stefan Roitsch,[‡] Joachim Mayer,[‡] and Alexander Böker^{*,†}

[†]DWI an der RWTH Aachen e. V., Lehrstuhl für Makromolekulare Materialien und Oberflächen, RWTH Aachen University, D-52056 Aachen, Germany

[‡]Gemeinschaftslabor für Elektronenmikroskopie, RWTH Aachen University, Ahornstr. 55, D-52074 Aachen, Germany

Supporting Information

ABSTRACT: Corrugated SiCN ceramic substrates fabricated by a facile replication process using nonlithographic PDMS masters were employed for the directed assembly of block copolymer microdomains. During thermal annealing of polystyrene-*b*-polybutadiene diblock copolymer, the material transport was guided by a wrinkled substrate to form regular modulations in the film thickness. As a consequence of the thickness-dependent morphological behavior of cylinder forming block copolymer, the film surface appears as sequenced patterns of alternative microphase-separated structures. The ordering process is attributed to the formation of inverted terraces which match the substrate topography, so that the resulting surface patterns are free from the surface relief structures within macroscopically large areas. The issues of the film thickness, the substrate surface energy, and the pattern geometry are addressed. Our approach demonstrates an effective synergism of external confinement and internal polymorphism of block copolymers toward complex hierarchically structured patterned surfaces.



INTRODUCTION

Self-assembly of block copolymers is a promising and low-cost route toward fabrication of hierarchically structured functional surfaces and patterns.^{1–6} Depending on a number of well-established internal and external parameters,^{7–11} block copolymers in thin films are guided to microphase separate into uniform microdomains with tunable dimensions and shapes including spheres,^{12,13} cylinders,^{14–16} lamellae,^{17–19} hybrid structures,^{20,21} or interconnected networks.^{22,23} Along with ABC terblock polymers²⁴ and complexed block copolymers,^{22,25} asymmetric cylinder-forming diblock copolymers exhibit structural polymorphism in confined geometries.^{11,26,27} The technological use of nanostructured block copolymer patterns depends decisively on our ability to ultimately manipulate their shape, the macroscopically uniform orientation, and long-range lateral order.

In the past years, intensive research convincingly demonstrated the possibility of precise registration of microphase-separated structures by using lithographically fabricated topographical²⁸ (known as graphoepitaxy)¹³ or/and chemical patterns.^{29–31} While chemical patterns take an advantage of a strong difference in the surface interactions of block copolymer component with the substrate patterns,³⁰ topographical graphoepitaxy in a form of regular^{32–34} or irregular substrate corrugations³⁵ imposes an additional confinement to the system and thus affects the microphase separation mechanism.

A diversity of topographic geometries has been used for microdomain registration ranging from randomly roughened

substrates,³⁵ trapezoidal shaped-Si grating substrates,³³ directional V-shaped grooves,³⁶ sawtoothed,³⁷ or channel topography^{13,32,38} up to lithographically fabricated regular posts²⁸ or holes.³⁹ Different criteria of the substrate topography have been introduced, including the ratio of the characteristic lateral periodicity of the pattern λ_s to the microdomain dimension L_0 ,³⁴ the ratio of λ_s to the film thickness,⁴⁰ and the ratio of λ_s to the root-mean-square vertical displacement of the surface topography R ,³⁵ as well as the ratio of the grating height to L_0 .³³ Ideal grating substrates (of $q_s R \sim 0.15$, where $q_s = 2\pi/\lambda_s$) gave rise to a lateral ordering of perforations in lamella along the peaks with corrugation amplitude of about $L_0/2$.³⁴ Sivaniah et al. demonstrated the appearance of perpendicular lamellae on rough substrates and found a critical surface roughness, below which the parallel orientation of lamella is favored.³⁵ Li et al. systematically studied modulations at the free surface in lamella-forming PS-P2VP diblock and triblock copolymer films supported by Si gratings with the heights which are comparable with the lamella period.³³ They determined topographical conditions for either in-phase (conformal) or out-of-phase (anticonformal) terrace formation. Relatively large aspect ratio grating substrates have been used to laterally align sphere-forming,¹³ and cylinder-forming block copolymers,⁴¹ and the mechanism of ordering in these cases was attributed to

Received: December 2, 2011

Revised: February 9, 2012

Published: February 22, 2012

the coordinated surface-field-directed wetting of the base and of the side walls of the gratings. Grating substrates have been successfully used to generate micrometer-scale periodic structures from PS-*b*-PMMA block copolymer: the standing-up and lying-down cylinders assembled periodically as a result of the film thickness-dependent surface morphology.³² The authors confirmed the importance of the compliance of the cylinder size to the trough width. However, uncontrolled dewetting and terracing of the film reduced the perfection of these patterns.³² Another strategy for generating regions from microphase-separated block copolymer structures have been employed by Bosworth et al.,⁴² who utilized a three-step approach based on selective solvent and block-selective solvent annealing with an intermediate UV cross-linking step to lock the structure at selectively masked areas.

Following the idea of Fasolka et al. on mediating sequenced patterns by substrate topography,³⁴ we take advantage of a macroscopic topographic parameter which matches the free surface profile of equilibrated block copolymer films. The phenomenon of spontaneous roughening of the film surface upon the equilibration of in-plane aligned microdomains (often referred to as “terrace formation”) has been long studied in regards to the dynamics of microdomain evolution.^{18,19,43} The shape of the transition region between the terraces depends greatly on the molecular weight and on the Flory–Huggins interaction parameter χ (i.e., on the chemical composition of the block copolymer as well as on the experimental variables which affect χ). From the practical point of view, the uncontrolled surface roughening of block copolymer films limits their applications in electronics, optics, and sensor technology.

In this work, we report a facile lithography-free method to overcome the problem of surface roughening and at the same time to generate ordered sequences from microphase-separated microdomains. Wrinkled SiCN (silicon carbon nitride) ceramic substrates have been fabricated by a replication process and were homogeneously covered with films of PS-*b*-PB diblock copolymer by floating. The corrugations dimensions of the substrates were in the range of the terrace shapes; i.e., they match the profile of the transition thickness between neighboring terraces of annealed PS-*b*-PB films. We first compare the morphological behavior of PS-*b*-PB films on flat and on corrugated substrates both under strong and under neutral surface fields. Further, the pattern formation as a function of the film thickness is discussed. Next, using grating substrates with a gradient in grating periodicity and amplitude, we demonstrate the importance of the compliance of the substrate corrugations with the characteristic roughness of the “terraced” film in order to eliminate the surface roughening on macroscopically large areas.

EXPERIMENTAL SECTION

Fabrication of Corrugated SiCN Ceramic Substrates. The nanostructured corrugated PDMS masters were prepared following an earlier described procedure.^{44,45} Thermally cross-linked PDMS pieces were initially mounted on a custom-made stretching apparatus and subsequently stretched uniaxially to a strain of 5% of their original length. These stretched PDMS pieces were oxidized for 490 s in air plasma (0.2 mbar, 100 W, Plasma Activate Flecto 10 USB). A hard silicon oxide layer forms regularly corrugated patterns on the PDMS surface when the stress is relaxed. Poly(vinylsilazane) (PVSZ, HTT 1800, KiON Corp.) was used as a SiCN ceramic precursor. 1 wt % of photoinitiator (Irgarcure 500, Ciba specialty) and 0.5 wt % of thermal initiator (dicumyl peroxide, Aldrich) were added to the polymer and homogeneously mixed by stirring for 10 min. The corrugated PDMS

surface was coated with trichloro(1H,1H,2H,2H-perfluorooctyl)silane ($(CF_3(CF_2)_5CH_2CH_2SiCl_3$, Aldrich) to avoid adhesion between master and polymer by the evaporation method under vacuum. The PDMS master was placed on a PVSZ thin film spin-coated at 1500 rpm for 45 s. Prior to spin-coating the polymer on a Si wafer substrate (CrysTech Inc.), the polymer was diluted to 30 wt % with propylene glycol monomethyl ether acetate (PGMEA, Sigma-Aldrich) to prevent cracks in the patterned ceramic surface induced by anisotropic shrinkage behavior during pyrolysis. To intrude the polymer effectively into the grooves of the PDMS master, vacuum was applied for 10 min. The solidified PVSZ replica was created by UV curing for 15 min (Panacol UV-F 400 F, 450 W, $\lambda = 325\text{--}380\text{ nm}$) without pressure. After peeling of the PDMS master, the cured PVSZ replica was annealed in a furnace at 800 °C under a nitrogen atmosphere for 2 h at a heating rate of 2 °C min⁻¹ to produce a SiCN ceramic material.⁴⁶ In order to prepare a neutral corrugated ceramic surface, a $29 \pm 1\text{ nm}$ carbon layer was evaporated onto the ceramic substrate using a sputter coater (S150B, Edwards). To obtain the planar SiCN ceramic substrate, a 30 wt % polymer solution diluted with PGMEA was spin-coated onto Si wafer at 1500 rpm for 45 s. UV-cross-linking and pyrolysis were then applied as described above.

Fabrication of SiCN Ceramic Substrate with Gradient of the Corrugations. Cross-linked PDMS was cut in substrates of $0.5 \times 3\text{ cm}^2$. To induce the surface pattern, the substrate is clamped in a custom-made stretching apparatus and stretched to 130% of its original length. A rectangular silicon wafer ($0.5 \times 0.7\text{ cm}^2$) with a spacer (glass slide with thickness of 1 mm) which is attached to one end was placed in the middle of the stretched sample. At one end, the wafer is resting directly on the sample, while at the opposite end a distance of 1 mm between the sample and the wafer is fixed. After exposure to the air plasma for 450 s at 0.2 mbar (Plasma Activate Flecto 10 USB, 100 W) the silicon wafer was removed prior to slow relaxation of the sample. For further use, the samples were placed on glass supports. Details of the preparation of the PDMS stamps with gradient of the corrugations and their characterization will be published elsewhere. To produce the SiCN ceramic replica from the gradient of the corrugations, fabrication steps including the UV-cross-linking and the pyrolysis were applied as mentioned above.

Preparation of Block Copolymer Thin Films. A poly(styrene-*b*-butadiene) ($M_{nPS} = 13.6\text{ kg/mol}$ and $M_{nPB} = 33.7\text{ kg/mol}$) (PS-*b*-PB, Polymer source Inc.) block copolymer with a total molecular weight of 47.3 kg/mol and polydispersity index of 1.03 was used in this work. 1 wt % toluene solution was prepared with the addition of stabilizer (2,6-di-*tert*-butyl-*p*-cresol) in an amount of 0.03 wt % of the polymer weight to prevent cross-linking of PB during thermal annealing. Thin films on flat silicon wafers, SiCN ceramic films and mica substrates (Plano GmbH) have been prepared by spin-coating with 1000, 2000, and 4000 rpm to produce PS-*b*-PB films with 70, 40, and 24 nm thickness, respectively. Prior to use, Si wafers and SiCN ceramic substrates were cleaned in toluene for 1 day, followed by snow jet and air plasma for 1 min at 0.2 mbar. Mica was freshly cleaved before film deposition.

In order to prepare a homogeneous polymer film on a corrugated substrate, a spin-coated film was floated from mica onto water surface and then picked up by the corrugated ceramic substrate. To equilibrate the microphase-separated structures, films have been thermally annealed under vacuum at 120 °C for 18 h.

Characterization. The nanostructured corrugated ceramic substrates, microdomain morphologies, and absolute film thicknesses of PS-*b*-PB were characterized by scanning force microscopy (SFM) in TappingMode with Bruker Dimension ICON AFM using OTESPA tips with a resonance frequency in the range of 278–357 kHz and a spring constant of 12–103 N/m. The characteristic surface topography in annealed PS-*b*-PB films was investigated using an optical microscope (Axioplan 2 imaging, ZEISS). The PS-*b*-PB film thicknesses on corrugations were measured by cross-sectional transmission electron microscopy (TEM). Samples for cross-sectional TEM measurements were prepared on a dual-beam FIB workstation (FEI Helios Nanolab). Prior to inserting the sample in the FIB, a thin Au layer was sputter-deposited on the surface of the sample to protect the polymer in the subsequent preparation steps. In addition, a thicker

Pt layer was e-beam-deposited in the FIB on the areas from which cross-sectional lamellae were extracted. The FIB lamellae were extracted via in situ lift-out and attached to an Omniprobe grid via Pt deposition.

RESULTS AND DISCUSSION

Asymmetrical block copolymers in thin films are known to show a rich phase behavior with deviations from the bulk structures. Although it is a potentially useful property, the sequences of morphological structures are in most cases observed at the thickness gradients when the microdomains have to adjust to the changing thickness,²⁶ or phase transitions occur very locally under strong interactions with the substrate.⁴⁷ The phase behavior of cylinder-forming polystyrene (PS)-*b*-polybutadiene (PB) diblock copolymer (PS-*b*-PB) on flat strongly and weakly interacting substrates under both thermal⁴⁷ and solvent annealing¹¹ has been intensively studied before. Earlier it was shown that on freshly cleaned silicon oxide substrates (silicon wafers) the formation of the in-plane cylinder phase (C_{\parallel}) as well as of the nonbulk perforated lamella (PL) and lamella (L) phases in PS-*b*-PB melts depends on the local film thickness.

Figure 1 displays the macroscopic surface features (a) and microphase-separated domains (b) of PS-*b*-PB on a flat SiCN

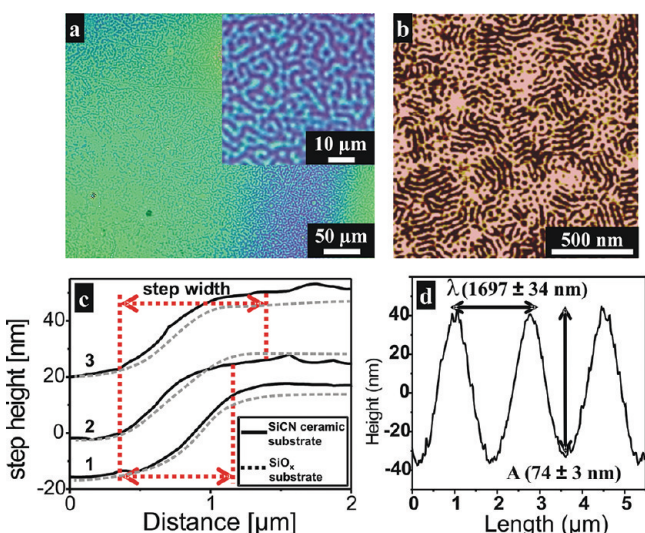


Figure 1. (a) Optical microscopy image of a 24 nm thick PS-*b*-PB film annealed on a flat SiCN ceramic substrate. The two colors correspond to two distinct film thicknesses. (b) SFM phase image of the same film. (c) Cross-section plot of SFM topography data, representing step height and step width between neighboring terraces in thermally annealed PS-*b*-PB films on flat silicon wafers (from ref 47) and on flat SiCN ceramic substrates. The number of a lower terrace (number of layers) is indicated. (d) SFM height profile of the corrugated SiCN ceramic substrate.

ceramic substrate after thermal annealing. The film shows a clear terrace formation behavior which is characteristic for strong surface fields at the substrate. Also, the microphase-separated pattern—a fine coexistence of C, PL, and L patches—confirms the strong pinning of the majority PB block to the SiCN ceramic surface and, consequently, reduced chain mobility in the bottom layer.⁴⁷ Both patterns—surface topography and microdomains—suffer from a low degree of order and small grain sizes. A detailed thickness-dependent morphological behavior of PS-*b*-PB on SiCN ceramic and

silicon oxide substrates is presented in Figures S1 and S2 (Supporting Information).

Despite an apparent randomness, the surface relief structures in Figure 1a and Figure S1 can be characterized by a certain characteristic periodicity which is the repeated step height (ca. 24–30 nm) and the step width (ca. 0.6–1.2 μm) where the indicated ranges slightly depend on the number of layers and on the substrate chemistry (Figure 1c). In the following, we study the phase behavior of PS-*b*-PB films on corrugated SiCN substrates (Figures 1d and 2) with the surface undulations

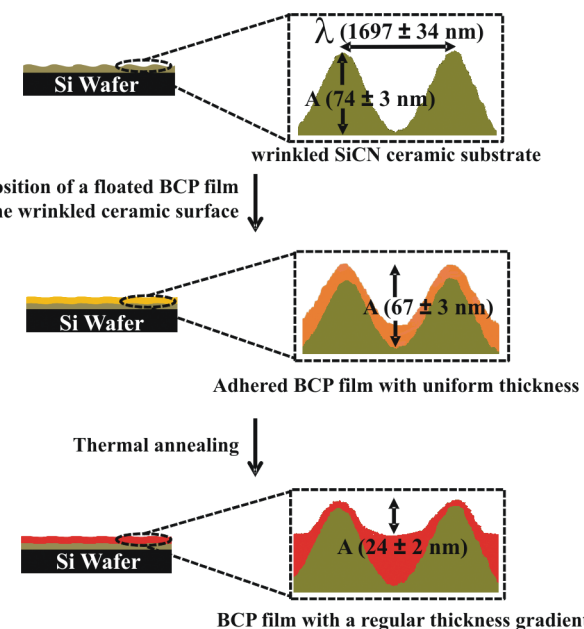


Figure 2. Schematic illustration of the substrate topography, the deposition of a homogeneous block copolymer film, and the development of thickness gradient in the film upon thermal annealing. Note that the height profiles on the right are measured cross sections from SFM height images.

which match the characteristic dimensions of the terraces (corrugation amplitude $A \sim$ tens of nm and corrugation wavelength λ (period) \sim order of μm).

These SiCN substrates are obtained by a facile replication process using nonlithographic PDMS masters with regular periodic patterns on a several mm² scale and are resistible to high temperature and most of the solvents which enables block copolymer processing via thermal- or solvent-annealing. The dimensions of the corrugated ceramic structures depend on the dimensions of the PDMS master as wells as on unavoidable shrinkage of the precursor material during the pyrolysis step. A detailed characterization of corrugated SiCN ceramic substrates replicated using PDMS masters has been reported earlier.⁴⁶

Phase Behavior on Strongly Interacting Corrugated Substrates. Figure 2 illustrates the sample preparation on corrugated substrates. The procedure includes a transfer of the spin-coated films via floating from mica to a water surface and then deposition onto the wrinkled ceramics followed by thermal annealing under vacuum. The floated block copolymer film completely adheres to the corrugated substrates so that the corrugations amplitude and wavelength exhibit no considerable changes. (Note that the height profiles in Figure 2 are real cross sections from SFM height images.) In contrast, thermal annealing significantly reduces the corrugations amplitude due

to the flow of the polymer melt into the grooves (Figure 2). Such redistribution of polymer material is in agreement with earlier studies of block copolymers on corrugated patterned surfaces.^{48–50}

The microphase-separated behavior of the samples prepared in the above way has been studied with SFM. Figure 3a,b displays the topography and phase images of a 24 nm thick PS-*b*-PB film (an initial spin-coating thickness on mica substrate) before the thermal annealing on the corrugated substrate. The initial corrugation amplitude (74 ± 3 nm) is slightly reduced after the adhesion of the film (67 ± 3 nm) (inset in Figure 3a) presumably due to a slight elastic deformation of the PS-*b*-PB material. The phase image in Figure 3b shows a disordered microphase separated structure which is a typical pattern after spin-coating. This confirms that the floating and adhesion steps do not affect the microphase separation.

Figure 3c–e presents the phase behavior after the annealing on the corrugated substrate. The corrugations in the height image (Figure 3c) have sharper edges as compared to the nonannealed film (Figure 3a) due to the flattening of the film in the valleys (as seen from the cross section of the corrugation profile in inset in Figure 3c). The amplitude of the profile is reduced to 24 ± 2 nm. As seen in Figure 3d, the initially disordered pattern developed after annealing into a sequence of distinct morphologies which follow the topography of the substrate. A featureless white pattern which is attributed to the PS sheet of the in-plane L phase (Figure 3e) is generated in the valleys of the corrugations, while the white (PS) lying cylinders (C_{\parallel}) are confined to the hills. This former cylinder phase is clearly distinguishable by the width of the white stripes from the striped pattern at the curved side walls, i.e., at transition film thickness. The two striped structures (which have the same spacing between the next neighboring white stripes within the measurement resolution) are separated by a narrow region of the PL structures. We tentatively attribute the narrow white stripes to standing lamellae (L_{\perp}) or distorted cylinders (DC_{\parallel}) phases. The sketch in Figure 3e tentatively relates the observed morphologies to the thickness modulation in the annealed film. Remarkably, as a result of the sequencing, the topographic pattern appears on the phase image with a 2-fold multiplication (Figure 3c,d), which implies the potential of our approach toward creating a chemically and topographically patterned surfaces.

Figure 3f shows an optical microscopy image of the annealed film where topographic features of the underlying substrate are visible. A striking result is the absence of the macroscopic patterning of the block copolymer film surface, i.e., the suppression of the terrace formation. This issue will be discussed in detail later.

Shown in Figure 4 is the morphological behavior of PS-*b*-PB films with a thickness of 40 nm (a, b) and 70 nm (c, d) which have been annealed on the corrugated substrates with similar characteristics as those in Figures 1d and 3. Both thicknesses are incompatible with the characteristic microdomain dimension. In both films basically the same sequence of structures (Figure 4b,d) as in the 24 nm thick film (Figure 3) is observed. The tiny differences in the morphological behavior, such as the precise position of the phase boundaries (the width of the stripes of each phase) and the phase identification (L_{\perp} versus DC_{\parallel}), are currently under detailed investigation and go beyond the scope of the present work.

Insets in Figure 4a,c display the cross sections of the films after annealing. The corrugations amplitude is reduced from

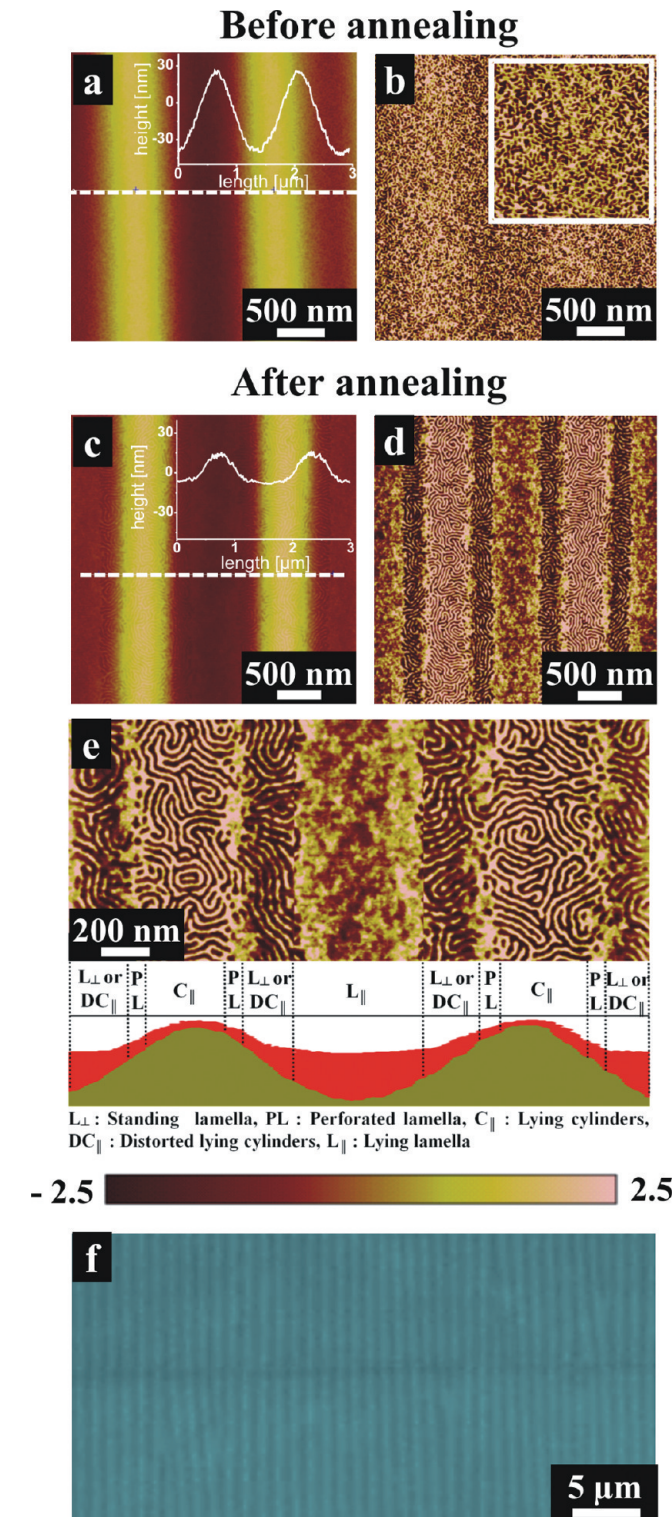


Figure 3. SFM height (a, c) and phase (b, d, e) images of a 24 nm thick PS-*b*-PB film (initial thickness after spin-coating on mica substrate): after deposition via floating onto a corrugated SiCN ceramic substrate (a, b) and after thermal annealing at 120 °C for 18 h (c–e) with the corresponding sketch showing a presumable assignment of the patterns to a particular morphology and film thickness. (f) Optical microscopy image of the film. Insets in (a) and (b) show cross-sectional height profiles along the indicated white dashed lines.

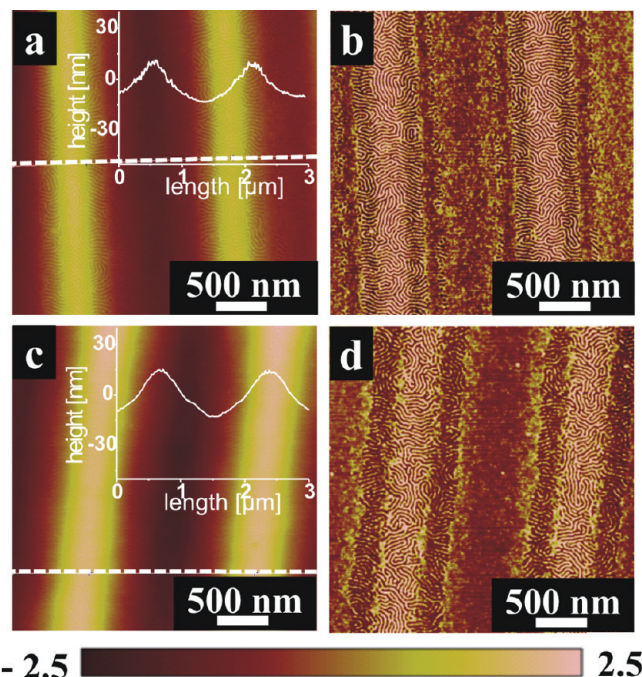


Figure 4. SFM topography (a, c) and phase (b, d) images of a 40 nm thick (a, b) and of a 70 nm thick (c, d) PS-*b*-PB film annealed on corrugated ceramic substrates at 120 °C for 18 h. Both thicknesses indicate the initial thickness of the films spin-coated on mica. Insets in (a) and (c) show cross-sectional height profiles along the indicated white dashed lines.

values of 64 ± 6 nm and 85 ± 6 nm after the films deposition to 24 ± 2 nm (Figure 4a) and to 28 ± 3 nm (Figure 4b), respectively. Importantly, the formation of terraces on corrugated substrates is also suppressed for these film thicknesses. We note that for all studied films the residual amplitude is in the range of 24–30 nm, which is very close to the intrinsic terrace step height in PS-*b*-PB films when they are thermally treated on flat substrates (Figure 1c).

Figure 5 shows a cross-sectional transmission electron microscopy (TEM) image of a thermally annealed PS-*b*-PB film with a nominal thickness of 70 nm (as in Figure 4c,d). It is clearly seen that the thickness of the film varies exactly between a minimum of 46 nm on the hills and a maximum of 86 nm in the valleys of the corrugations. However, the precise determination and assignment of the number of layers in the valleys and on the hills is only possible when the internal structure through the film is identified, since the interlayer period increases with the structure transformation from the cylinder phase to the PL phase and to the L phase.⁴⁷

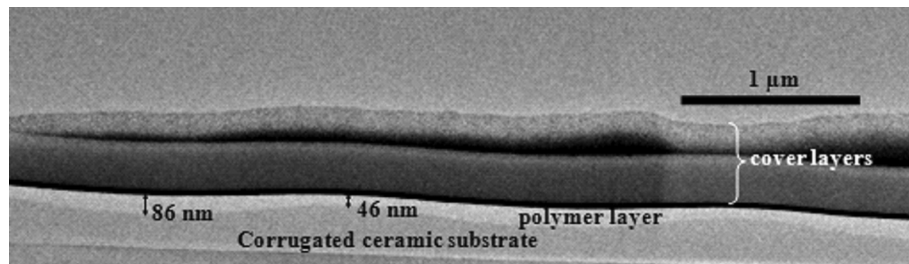


Figure 5. Cross-sectional TEM image of PS-*b*-PB film with 70 nm (initial spin-coating thickness on mica substrate) on corrugated SiCN ceramic substrate after thermal annealing at 120 °C for 18 h.

Phase Behavior on Weakly Interacting Corrugated Substrates. Neutrality of the block copolymer components to the substrate surface has been introduced by a thin carbon layer which was evaporated on the corrugated as well as on flat SiCN substrates. On weakly interacting carbon substrates, PS-*b*-PB exhibits asymmetric wetting conditions with the PB block at the free surface and no enthalpic preference for the components at the substrate. On flat carbon-coated substrates the morphological behavior is generally similar to that in bulk.⁴⁷ In order to satisfy the substrate neutrality, a bottom layer of half cylinders is stabilized on flat substrates, and all the following cylinder layers are aligned parallel to the film plane. The only phase transition from the bulk C_{||} morphology to the PL phase was observed around 1.5 layers thickness in the areas with the minor thickness variation.⁴⁷

Figure 6 displays the microphase separation behavior of a 40 nm thick film which has been prepared on a carbon-coated corrugated SiCN substrate in accordance with the procedure shown in Figure 2. The initial corrugation amplitude of the SiCN substrate is insignificantly reduced after the coating with carbon layer and with the polymer film (inset in Figure 6a). The phase image in Figure 6b shows a disordered microphase-separated pattern before thermal annealing which is the same as after floating onto the bare SiCN surface.

The phase behavior of the annealed samples on corrugated carbon-coated substrates is presented in Figure 6c–f. The in-plane C_{||} phase is observed in thinned parts of the film on the hills. In addition, the nonbulk L phase appears in the valleys (Figure 6e,f). In this case, the pattern multiplication is not achieved in the phase image (Figure 6e,d). The phase behavior in a thinner film (with 24 nm thickness) on carbon-coated corrugations exhibits the same sequence of morphologies which consists of alternating C_{||} phase (with single PL patches) and lying lamellae L phase (Figure S3, Supporting Information). However, the development of the L phase on corrugations is a newly observed feature as compared to the behavior on flat carbon-coated substrates. Although the in-plane L phase with the PB sheet at the free surface satisfies the wetting condition, the nonbulk morphology is an excited state which presumably is a consequence of the confinement induced by the corrugations.

Figure 6g presents an optical microscopy image of the annealed film. Similar to the strongly interacting SiCN ceramic corrugated substrates, the terrace formation is suppressed by the carbon-coated corrugations. Following this low-cost procedure, macroscopically structured surfaces with chemically patterned topographical channels could be produced.

Guided Terrace Formation in Thin Films on Substrates with Gradient of the Corrugations. An important

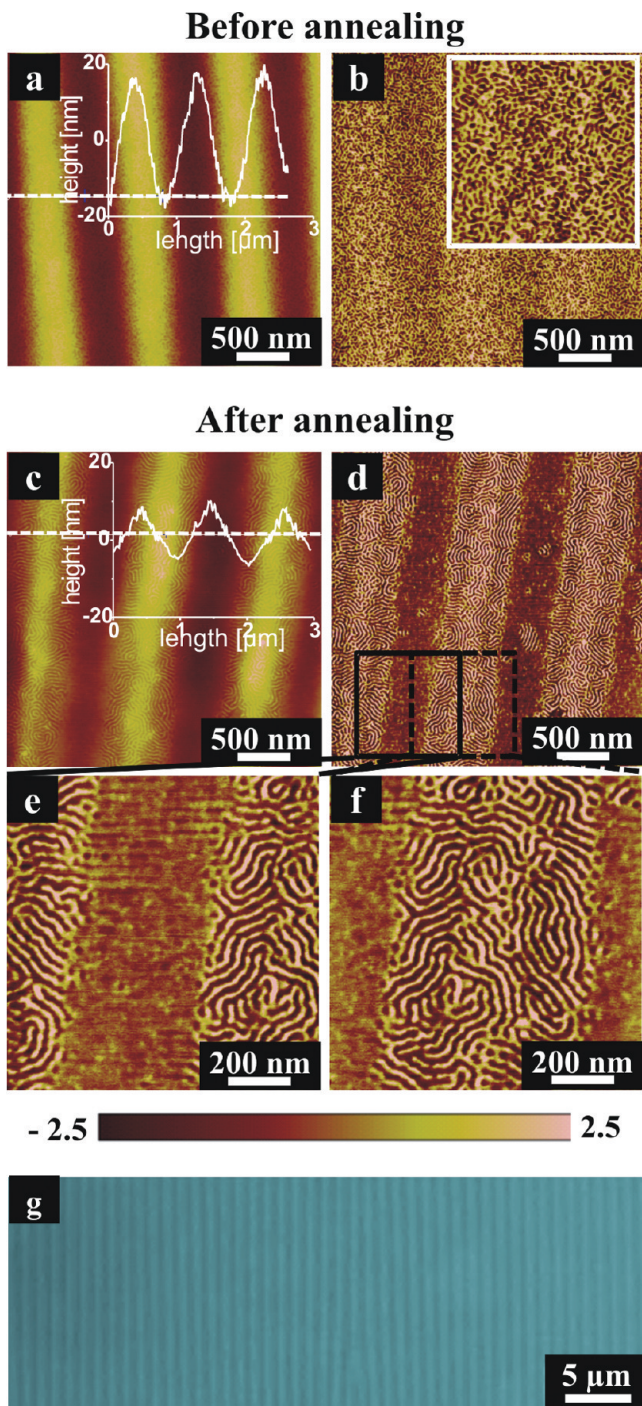


Figure 6. SFM topography (a, c) and phase (b, d, e, f) images of a 40 nm thick PS-*b*-PB film (initial spin-coating thickness on mica substrate): after floating onto a carbon-coated corrugated SiCN ceramic substrate (a, b); after thermal annealing at 120 °C for 18 h (c–f) and the optical microscopy image of the film (g). Insets in (a) and (c) show cross-sectional height profiles along the indicated white lines.

insight regarding the role of the corrugation geometry in suppressing the terrace formation was derived from the analysis of PS-*b*-PB films which have been annealed on ceramic substrates with gradient of the corrugations. Figure 7 presents optical microscopy and SFM images of a thermally annealed 24 nm thick PS-*b*-PB film on a wrinkled substrate with the corrugation amplitude A changing in the range from 55 to 16

nm and the corrugation wavelength λ changing in the range from ca. 1000 to ca. 700 nm (Figure 7a). We note that as the wrinkles are produced by relaxation of a stretched and surface-oxidized PDMS stamp where both the wrinkles' amplitude and the wrinkles' wavelength depend linearly on various parameters of the PDMS stamps (e.g., elastic moduli, silicon oxide film thickness), they cannot be varied independently from each other.⁵¹ As seen in Figure 7b–g, both the ordering of the microphase-separated structures and terracing of the film surface are related to corrugations dimensions. As compared to well-structured and terrace-free PS-*b*-PB films on the corrugations with $A \approx 55$ nm and with $\lambda \approx 1010$ nm which have been extensively described above (Figures 3, 4, 6, and 7b,e), the directing effect of the corrugations diminishes with decreasing A and λ . As soon as the surface relief structures (terraces) are allowed to be formed (Figure 7c), the sequencing of the microphase-separated patterns is significantly less pronounced. As seen in Figure 7f, the C_{||} phase and the PL phase alternate with interruptions, while the L phase has vanished completely. On smaller corrugations, terraces are built over the entire area (Figure 7d), and the microphase-separated structures are almost unaffected by the substrate topography (Figure 7g). We note that on the latter corrugations the PS-*b*-PB films still show a thickness-dependent morphological behavior since the microstructures in the neighboring terraces are different (highlighted by white border lines in Figure 7g). Since all gradient of the corrugations belong to one and the same substrate, we can exclude that the observed effects are affected by possible experimental perturbations related to the variations in the starting film thickness or the floating and annealing processes which may slightly differ from one to another experiment.

Since the variation in wavelength is inevitably accompanied by the variation in the amplitude, we used the roughness parameter $qA/2$, where $q = 2\pi/\lambda$ and A refers to the amplitude, to summarize the results. The corrugations in Figure 7b,c,d are characterized by roughness parameters of 0.16, 0.09, and 0.07, respectively. We believe that the near equality of the surface roughness parameter (0.16) of the perfectly guiding corrugations (Figure 7d,e) with that of the ideally grating substrates (0.15)³⁵ is accidental or a coincidence, since in earlier studies the roughness dimension were varied around the nanometer range. We rather use this value to compare it with the geometry of the intrinsic surface relief structures of PS-*b*-PB films on flat substrates,⁴⁷ i.e., with the step height H (ca. 25 nm) and the step width D (ca. 1 μm). The best fit to the perfectly guiding corrugations is obtained with $2\pi H/D$ (0.15). This result, on one side, gives a quantitative measure for the targeted fabrication of corrugations which eliminate the surface relief structures and, on the other side, suggests that the formation of sequenced patterns is a consequence of the “inverted terrace formation” under confinement by substrate corrugations.

CONCLUSIONS

We have demonstrated a facile and simple route to achieve sequenced patterns from microphase-separated structures in block copolymer films. For the guided block copolymer assembly we used structured corrugated SiCN ceramic substrates which were fabricated by a facile replication process using nonlithographic PDMS masters. Homogeneous block copolymer films have been floated onto to the corrugated substrate without significant changes to the corrugations topography. After thermal annealing, the polymer material is

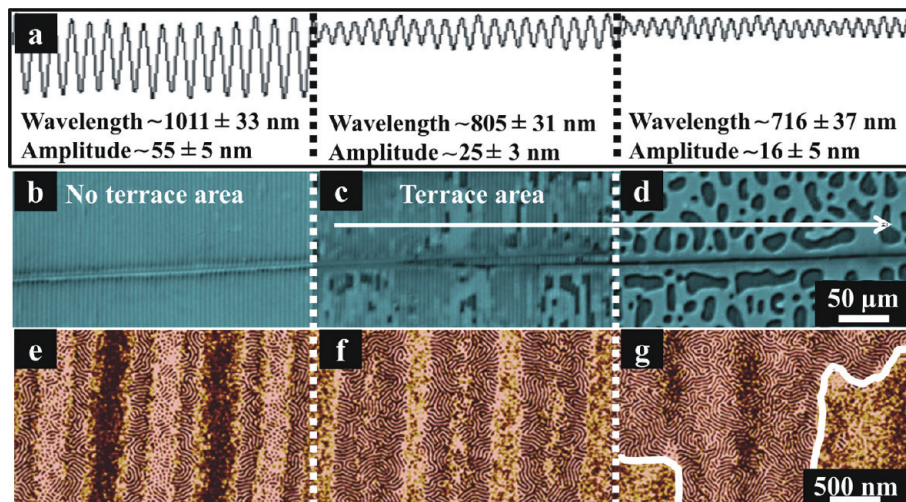


Figure 7. (a) Cross-sectional height profiles of the areas with gradient of the corrugations. (b, c) Optical microscopy and (c–g) SFM phase images of a 24 nm thick PS-*b*-PB film which has been floated onto the SiCN ceramic substrate with gradient of the corrugations and thermally annealed at 120 °C for 18 h.

redistributed between the hills and grooves of the corrugations. As a consequence of the thickness-dependent morphological behavior, the block copolymer is guided into sequenced patterns of alternative cylinder, perforated lamella, and lamella phases which follow the topography of the substrate. On strongly interacting corrugations, the phase pattern appears as a 2-fold multiplication of the initial topographic pattern. The position of the morphological boundaries as well as the stability of nonbulk morphologies is shown to be dependent on the film thickness, dimensions of the substrate corrugations, and the surface fields at the substrate. An important result is the suppression of the macroscopic roughening of the film surface (of terrace formation) so that the resulting microphase-separated patterns are free from the surface relief structures within macroscopically large areas. This phenomenon is attributed to the formation of inverted terraces when the substrate topography matches the dimensions of freely formed (on flat substrates) steps between neighboring terraces. Our approach demonstrates an effective synergism of external confinement and internal polymorphism of block copolymers toward complex hierarchically structured patterned surfaces.

■ ASSOCIATED CONTENT

S Supporting Information

Optical images of surface topography and SFM phase images of PS-*b*-PB films thermally annealed on planar surfaces and carbon-coated corrugated SiCN ceramic substrate. This material is available free of charge via the Internet at <http://pubs.acs.org>.

■ AUTHOR INFORMATION

Corresponding Author

*E-mail: tsarkova@dwi.rwth-aachen.de (L.T.); boeker@dwi.rwth-aachen.de (A.B.).

Notes

The authors declare no competing financial interest.

■ ACKNOWLEDGMENTS

The authors thank Clemens Liedel for support during the AFM measurements. S.P. acknowledges RWTH Aachen for a PhD fellowship.

■ REFERENCES

- (1) Park, C.; Yoon, J.; Thomas, E. L. *Polymer* **2003**, *44*, 6725–6760.
- (2) Li, M.; Coenjarts, C. A.; Ober, C. K. *Adv. Polym. Sci.* **2005**, *190*, 183–226.
- (3) Marencic, A. P.; Register, R. A. *Annu. Rev. Chem. Biomol. Eng.* **2010**, *1*, 277–297.
- (4) Darling, S. B. *Prog. Polym. Sci.* **2007**, *32*, 1152–1204.
- (5) Hamley, I. W. *Prog. Polym. Sci.* **2009**, *34*, 1161–1210.
- (6) Park, S.; Russell, T. P. *Nano* **2010**, *5*, 1–11.
- (7) Fredrickson, G. H.; Bates, F. S. *Annu. Rev. Mater. Sci.* **1996**, *26*, 501–550.
- (8) Hamley, I. W. *The Physics of Block Copolymers*; Oxford University Press: New York, 1998.
- (9) Matsen, M. W. *Curr. Opin. Colloid Interface Sci.* **1998**, *3*, 40–47.
- (10) Fasolka, M. J.; Mayes, A. M. *Annu. Rev. Mater. Res.* **2001**, *31*, 323–355.
- (11) Tsarkova, L.; Sevink, G. J. A.; Krausch, G. *Adv. Polym. Sci.* **2010**, *227*, 33–73.
- (12) Segalman, R. A.; Hexemer, A.; Kramer, E. J. *Macromolecules* **2003**, *36*, 6831–6839.
- (13) Segalman, R. A.; Yokoyama, H.; Kramer, E. J. *Adv. Mater.* **2001**, *13*, 1152–1155.
- (14) Radzilowski, L. H.; Carvalho, B. L.; Thomas, E. L. *J. Polym. Sci., Part B: Polym. Phys.* **1996**, *34*, 3081–3093.
- (15) Kim, H.-C.; Russell, T. P. *J. Polym. Sci., Part B: Polym. Phys.* **2001**, *39*, 663–668.
- (16) Knoll, A.; Magerle, R.; Krausch, G. *J. Chem. Phys.* **2004**, *120*, 1105–1116.
- (17) Collin, B.; Chatenay, D.; Coulon, G.; Ausserre, D.; Gallot, Y. *Macromolecules* **1992**, *25*, 1621–1622.
- (18) Coulon, G.; Russell, T. P.; Deline, V. R.; Green, P. F. *Macromolecules* **1989**, *22*, 2581–2589.
- (19) Maaloum, M.; Ausserre, D.; Chatenay, D.; Coulon, G.; Gallot, Y. *Phys. Rev. Lett.* **1992**, *68*, 1575–1578.
- (20) Harrison, C.; Park, M.; Chaikin, P.; Register, R. A.; Adamson, D. H.; Yao, N. *Macromolecules* **1998**, *31*, 2185–2189.
- (21) Elbs, H.; Drummer, C.; Abetz, V.; Krausch, G. *Macromolecules* **2002**, *35*, 5570–5577.
- (22) Meuler, A. J.; Hillmyer, M. A.; Bates, F. S. *Macromolecules* **2009**, *42*, 7221–7250.
- (23) Sperschneider, A.; Schacher, F. H.; Tsarkova, L.; Böker, A.; Müller, A. H. E. *Macromolecules* **2010**, *43*, 10213–10215.
- (24) Krausch, G.; Magerle, R. *Adv. Mater.* **2002**, *14*, 1579–1583.
- (25) van Zoelen, W.; ten Brinke, G. *Soft Matter* **2009**, *5*, 1568–1582.

- (26) Knoll, A.; Horvat, A.; Lyakhova, K. S.; Krausch, G.; Sevink, G. J. A.; Zvelindovsky, A. V.; Magerle, R. *Phys. Rev. Lett.* **2002**, *89*, 035501/1–035501/4.
- (27) Dobriyal, P.; Xiang, H.; Kazuyuki, M.; Chen, J.-T.; Jinnai, H.; Russell, T. P. *Macromolecules* **2009**, *42*, 9082–9088.
- (28) Bita, I.; Yang, J. K. W.; Jung, Y. S.; Ross, C. A.; Thomas, E. L.; Berggren, K. K. *Science* **2008**, *321*, 939–943.
- (29) Ruiz, R.; Kang, H.; Detcheverry, F. A.; Dobisz, E.; Kercher, D. S.; Albrecht, T. R.; de Pablo, J. J.; Nealey, P. F. *Science* **2008**, *321*, 936–939.
- (30) Park, S.-M.; Stoykovich, M. P.; Ruiz, R.; Zhang, Y.; Black, C. T.; Nealey, P. F. *Adv. Mater.* **2007**, *19*, 607–611.
- (31) Kim, S. O.; Solak, H. H.; Stoykovich, M. P.; Ferrier, N. J.; de Pablo, J. J.; Nealey, P. F. *Nature* **2003**, *424*, 411–414.
- (32) Sundrani, D.; Sibener, S. J. *Macromolecules* **2002**, *35*, 8531–8539.
- (33) Li, Z.; Qu, S.; Rafailovich, M. H.; Sokolov, J.; Tolan, M.; Turner, M. S.; Wang, J.; Schwarz, S. A.; Lorenz, H.; Kotthaus, J. P. *Macromolecules* **1997**, *30*, 8410–8419.
- (34) Fasolka, M. J.; Harris, D. J.; Mayes, A. M.; Yoon, M.; Mochrie, S. G. J. *Phys. Rev. Lett.* **1997**, *79*, 3018–3021.
- (35) Sivanah, E.; Hayashi, Y.; Matsubara, S.; Kiyono, S.; Hashimoto, T.; Fukunaga, K.; Kramer, E. J.; Mates, T. *Macromolecules* **2005**, *38*, 1837–1849.
- (36) Chuang, V. P.; Cheng, J. Y.; Savas, T. A.; Ross, C. A. *Nano Lett.* **2006**, *6*, 2332–2337.
- (37) Park, S.; Lee, D. H.; Xu, J.; Kim, B.; Hong, S. W.; Jeong, U.; Xu, T.; Russell, T. P. *Science* **2009**, *323*, 1030–1033.
- (38) Jung, Y. S.; Ross, C. A. *Adv. Mater.* **2009**, *21*, 2540–2545.
- (39) Xiao, S.; Yang, X.; Park, S.; Weller, D.; Russell, T. P. *Adv. Mater.* **2009**, *21*, 2516–2519.
- (40) Park, S.-M.; Berry, B. C.; Dobisz, E.; Kim, H.-C. *Soft Matter* **2009**, *5*, 957–961.
- (41) Sundrani, D.; Darling, S. B.; Sibener, S. J. *Nano Lett.* **2004**, *4*, 273–276.
- (42) Bosworth, J. K.; Black, C. T.; Obert, C. K. *ACS Nano* **2009**, *3*, 1761–1766.
- (43) Horvat, A.; Knoll, A.; Krausch, G.; Tsarkova, L.; Lyakhova, K. S.; Sevink, G. J. A.; Zvelindovsky, A. V.; Magerle, R. *Macromolecules* **2007**, *40*, 6930–6939.
- (44) Bowden, N.; Huck, W. T. S.; Paul, K. E.; Whitesides, G. M. *Appl. Phys. Lett.* **1999**, *75*, 2557–2559.
- (45) Stafford, C. M.; Harrison, C.; Beers, K. L.; Karim, A.; Amis, E. J.; Vanlandingham, M. R.; Kim, H. -C.; Volksen, W.; Miller, R. D.; Simonyi, E. E. *Nature Mater.* **2004**, *3*, 545–550.
- (46) Park, S.; Böker, A. *J. Mater. Chem.* **2011**, *21*, 11734–11736.
- (47) Tsarkova, L.; Knoll, A.; Krausch, G.; Magerle, R. *Macromolecules* **2006**, *39*, 3608–3615.
- (48) Jeong, S.-J.; Moon, H.-S.; Shin, J.; Kim, B. H.; Shin, D. O.; Kim, J. Y.; Lee, Y.-H.; Kim, J. U.; Kim, S. O. *Nano Lett.* **2010**, *10*, 3500–3505.
- (49) Sundrani, D.; Darling, S. B.; Sibener, S. J. *Langmuir* **2004**, *20*, 5091–5099.
- (50) Jung, Y. S.; Ross, C. A. *Nano Lett.* **2007**, *7*, 2046–2050.
- (51) Cerdá, E.; Mahadevan, L. *Phys. Rev. Lett.* **2003**, *90*, 074302/1–074302/4.

■ NOTE ADDED AFTER ASAP PUBLICATION

This article posted ASAP on February 22, 2012. Figure 5 has been revised. The correct version posted on February 23, 2012.